Nanoscale View of Alignment and Domain Growth in a Hexagonal Columnar Liquid Crystal

Shuoyuan Huang¹, Shinian Cheng², Jianzhu Ju², Debaditya Chatterjee¹, Junguang Yu³, Harald Bock⁴, Lian
 Yu³, Mark Ediger², Paul M. Voyles^{1,*}

- Department of Materials Science and Engineering, University of Wisconsin Madison, Madison, Wisconsin 53706, USA
- ²Department of Chemistry, University of Wisconsin Madison, Madison, Wisconsin 53706,
 USA
- ³Department of Pharmacy, University of Wisconsin Madison, Madison, Wisconsin 53706,
 USA
- 4Centre de Recherche Paul Pascal, Univerisité de Bordeaux & CNRS, 33600 Pessac,
 France

Abstract Highly ordered liquid crystalline (LC) phases have important potential for organic electronics. We studied the molecular alignment and domain structure in a columnar LC thin film with nanometer resolution during *in situ* heating using four-dimensional scanning transmission electron microscopy (4D STEM). The initial disordered vapor-deposited LC glass thin film rapidly ordered at its glass transition temperature into a hexagonal columnar phase, with small (< 10 nm), well-aligned, planar domains (columns oriented parallel to the surface). Upon further heating, the domains coarsen via bulk diffusion, then the film crystallizes, then finally transforms back to a LC phase at even higher temperature. The LC phase at high temperature shows remarkably straight columns of molecules, which we attribute to structure inherited from the intermediate crystalline phase. Nanoscale 4D STEM offers unique insight into the mechanisms of domain reorganization, and intermediate crystallization is a potential approach to manipulate orientational order and texture at the nanoto mesoscale in LC thin films.

Keywords: Liquid crystals, *in situ* transmission electron microscopy, nanoscale ordering, domain growth, phase behaviors

Introduction

1 2

13

14

15 16

17

18

19

20

21

22

23 24

25

26

27

- 29 Liquid crystalline (LC) materials have been widely engineered for organic semiconductor devices.
- 30 Anisotropic structures in LC lead to unique anisotropic electronic and optoelectronic properties¹⁻⁴. The
- 31 charge mobility in the columnar phase of a discotic LC is typically a few orders of magnitude higher along
- 32 the column direction than that normal to the column⁵. Homogeneous or heterogeneous interfaces in organic
- 33 semiconductors can also significantly influence charge transport behavior^{6,7}. On a broader device level, the
- 34 performance of organic electronics and photonics relies on careful engineering of the microstructure.
- 35 Extensive efforts have been made to manipulate patterned topological defects⁸ or alignment^{9,10}. Controlling
- both the nanoscale orientational order and the microstructural texture is critical for various applications^{11–}
- 37 ¹⁴, but direct measurement of orientational order, especially at the nanoscale, has been difficult.
- 38 LC phases have been found to undergo glass transitions^{15–17} and physical vapor deposition (PVD) can be
- 39 used to synthesize glassy LC thin films with controllable structural order¹⁸. Previous research has shown
- 40 that by varying deposition conditions, thin films of phenanthro[1,2,3,4-ghi]perylene-1,6,7,12,13,16-
- 41 hexacarboxylic 6,7,12,13-tetraethyl, 1,16-dimethyl ester (hereafter called phenanthroperylene-ester) can be

obtained with either homeotropic alignment, in which the disc-like molecules are parallel to the substrate, or planar alignment, in which the discs are perpendicular to the substrate¹⁹. Independent of alignment, molecules organize into a hexagonal columnar phase via π - π stacking. Which alignment forms depends on whether the system has sufficient surface mobility and surface residence time during deposition to find a low enthalpy structure²⁰ resulting from the lower interface energy at the free surface of planar orientation compared to homeotropic²¹. The surface mobility mechanism was tested by four-dimensional scanning transmission electron microscopy (4D STEM) measurement of the nanoscale domain sizes, which were connected quantitatively to the surface diffusivities for films grown at different substrate temperatures²². The alignment in discotic LC reacts to external stimuli²³, and since it is thermotropic, the alignment in vapor deposited thin films can be further manipulated through thermal annealing²⁴.

Here we use *in situ* 4D STEM experiments to study the evolution of microstructure in a discotic LC with unprecedented, nanometer resolution. Starting with a glassy phenanthroperylene-ester film, we investigate the changes in local orientational order that occur during continuous heating. 4D STEM can be used to probe localized structural order in non-crystalline materials^{25,26}. Low-dose 4D STEM with an ultrafast detector²⁷ is an excellent method to probe nano- and mesoscale structural order in beam-sensitive materials^{28–30}. Upon heating, we find that initially disordered phenanthroperylene-ester films develop planar alignment near the glass transition temperature (392 K), with hexagonal LC domains quickly extending through the thickness of the film. With further heating, domains grow laterally and then start to crystallize. Finally, the partially crystallized film melts to an LC phase that exhibits much straighter intradomain texture than the lower temperature LC structure. We propose a mechanism for domain coarsening based on bulk diffusion, which stands in contrast to dominance of surface diffusion on domains during film growth.

Results and Discussion

 The phenanthroperylene-ester films exhibit three basic types of diffraction patterns as a function of temperature. At room temperature and from 360 K to 380 K, the diffraction patterns exhibit amorphous diffraction in complete, isotropic rings, as shown in Fig. 1a. This suggests the film is in a glassy state with disordered molecular alignment, as expected from the deposition conditions. Starting at 395 K, the rings transform into a pair of opposing arcs at $k = 0.28 \text{ Å}^{-1}$ and particular azimuthal angles, as shown in Fig. 1b. The arcs correspond to the direction of π - π stacking along the columns in the columnar LC phase. By 460 K, the arcs have transitioned into diffraction spots characteristic of crystalline phenanthroperylene-ester in a fraction of diffraction patterns, as shown in Fig. 1c.

Figure 1d shows orientation maps of the π - π stacking directions in phenanthroperylene-ester thin films on continuous heating from 395 K to 480 K. Mapping results from additional experiments on different regions are shown in Fig. S3. Starting from the emergence of π - π diffraction are at 395 K, the orientation domains grow laterally with increasing temperature. The microstructure of orientation shows typical planar LC texture from 400 K to 425 K, similar to as-deposited PVD films grown at 370 K to 392 K²². Starting from 430 K, large orientation domains with uniform intradomain orientation start to form. Those domains occupy the entire field of view at 450 K and above. These large domains show sharp transitions of column orientation from one domain to another, unlike the gradual change of orientations in the smaller domains at lower temperatures. Sharp spot diffraction patterns like Fig. 1c are detected in some but not all of these larger domains at temperatures down to 430 K.

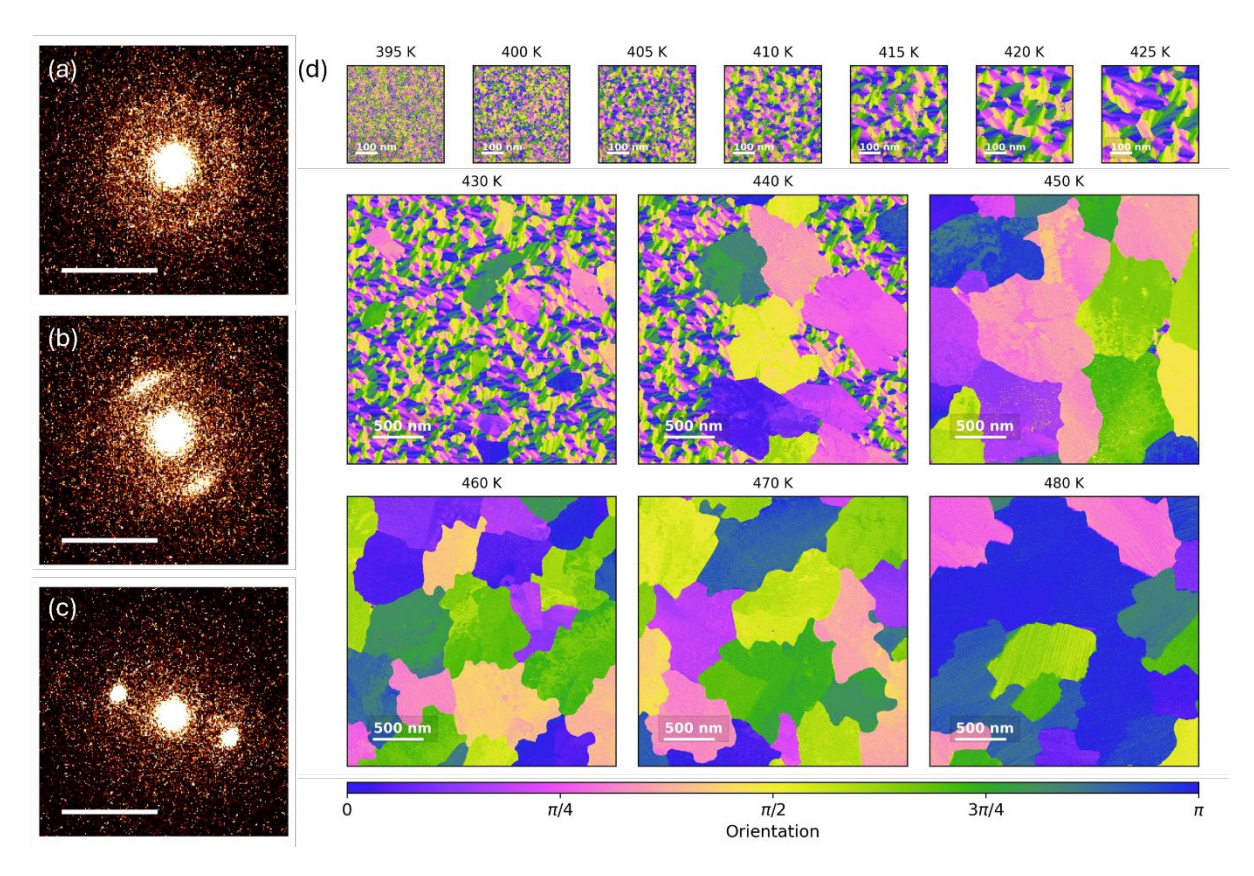


Figure 1. Example diffraction patterns of (a) disordered glass at 360 K, (b) planar LC at 400 K, and (c) crystal at 460 K for phenanthroperylene-ester thin film. (d) Orientation maps of the thin film during with continuous heating from 395 K to 480 K with a heating rate of 1 K/min. Displayed patterns in (a-c) are binned in space by 4 to decrease noise and enhance the diffraction features. Scale bars in (a-c) are 0.5 Å⁻¹. Maps in (d) are acquired from different regions at each temperature.

The lateral domain size can be estimated from the orientation correlation function^{22,30} calculated from the orientation maps as a function of spatial distance Δr and misorientation angle $\Delta \phi$:

$$C(\Delta r, \Delta \phi) = \frac{\langle I(r, \phi)I(r + \Delta r, \phi + \Delta \phi)\rangle_{r, \phi}}{\langle I(r, \phi)\rangle_{r, \phi}^{2}}.$$
 (1)

 $C(\Delta r, \Delta \phi)$'s calculated from orientation maps in Fig. 1d are shown in Fig. S4. C=1 corresponds to randomly distributed Δr and $\Delta \phi$. Therefore, C>1 near the origin represents strong intradomain ordering. As LC diffraction arcs appear at 395 K, $C(\Delta r, \Delta \phi)$ does not show significant ordering until 400 K. This is because the orientation domains are too small at 395 K to create any correlation. Above 440 K, the domains become too large to capture their statistics inside one field of view, creating non-random correlation at large distance and misorientation. The distance at which orientation correlation function $C(\Delta r, \Delta \phi = 1^{\circ})$ decays to 2 can be defined as a correlation length ξ to approximate the domain size²², as illustrated in Fig. S5. Figure 2a shows the quantified lateral domain size from orientation maps acquired at different temperatures. Similar to the qualitative observation from Fig. 1d, the domain size increases from \sim 10 nm at 400 K, just above spatial resolution of the measurement, to \sim 60 nm at 430 K, before an abrupt increase to 500 \sim 1000 nm between 430 K and 440 K. The domain size is constant within experimental uncertainty at 440 K and above. This abrupt increase is evidently a direct result of the emergence of large domains with uniform orientation.

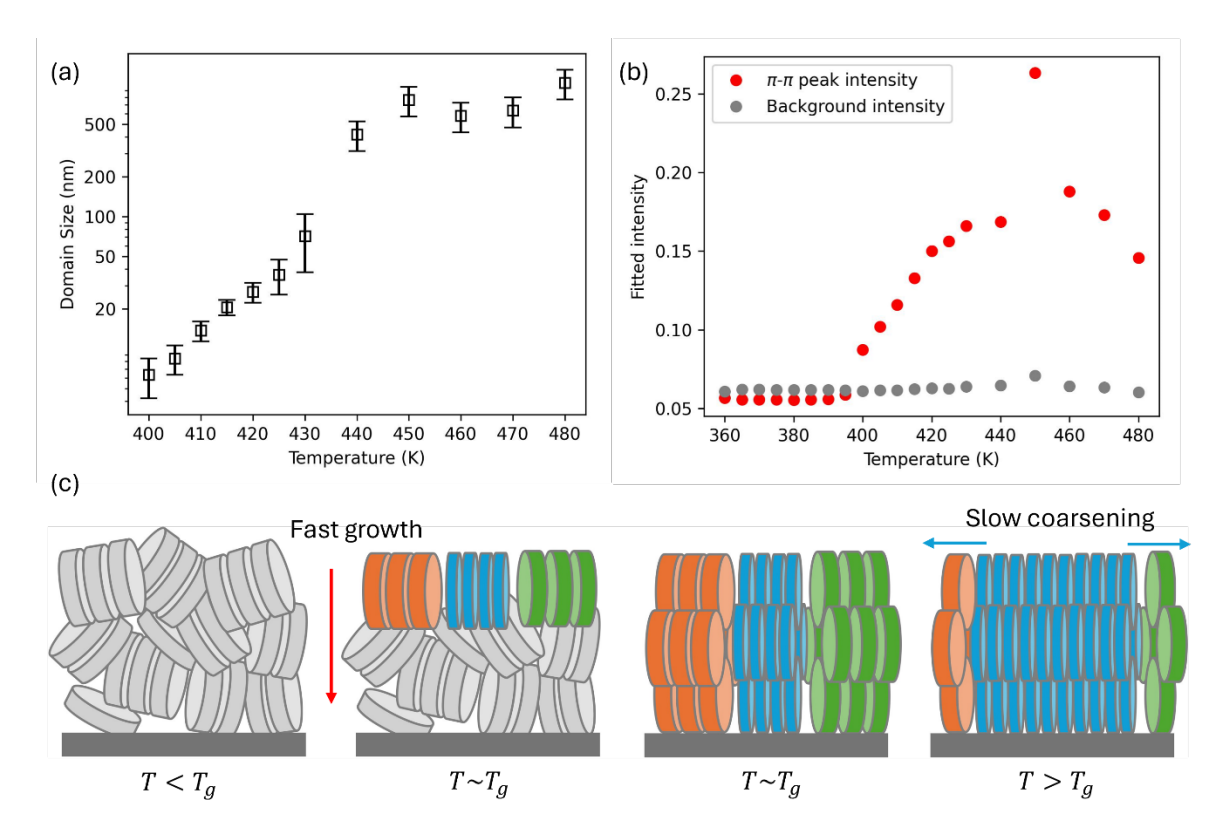


Figure 2. (a) Lateral domain size from orientation correlation functions as a function of temperature. Error bars from 400 K to 440 K are standard deviation of domain size calculations from four subdivisions of the field of view at each temperature. The domain size is too large above 440 K for subdivision, so the error bars are set to the average fractional error of the lower temperature data. (b) Average fitted π - π peak and background intensities of the azimuthal diffraction profiles at different temperatures. (c) Scheme of formation of oriented domains of hexagonal LC and their coarsening in the thin film during continuous heating. Gray molecules represent disordered glass and colored molecules represent planar-oriented hexagonal LC domains with different in-plane orientations. Molecules are not drawn to scale.

At temperatures near T_g , the lateral domain sizes are smaller than the 40 nm film thickness. However, only one set of diffraction arcs is observed in each diffraction pattern, so only a single orientation domain exists throughout the thickness at a given probe position. This microstructure suggests two pathways for vertical, through-thickness domain growth: (1) a small planar nucleus forms near either the film-substrate or the film-vacuum interface and grows by consuming disordered regions with a vertical growth rate similar to the lateral growth rate; or (2) after formation of nucleus near either interface, the vertical growth happens at a high growth rate, such that the vertical domains fill the thickness faster than the experimental time scale, and the newly nucleated domains "instantly" extend throughout the film. In pathway (1), the background intensity, which primarily comes from diffuse scattering of the disordered glass state, would decrease with increasing π - π peak intensity, as the disordered alignment was consumed by the planar one. Figure 2b shows the measured average π - π peak intensities and background intensities as functions of temperatures. The background intensity stays constant with temperature, so pathway (2) is most likely correct. Elongated domains that span the thickness are observed at 395 K as soon as planar alignment develops.

Figure 2c illustrates the scenario of planar domain formation and coarsening. The as-prepared film consists of non-hexagonal packing of π - π stacked columns with random in-plane orientation, creating the diffuse isotropic diffraction pattern seen in Fig. 1a. The molecules are close to planar alignment as evidenced by a

moderately high birefringence determined from deposition rate-temperature superposition¹⁹. At the glass transition temperature, the molecules obtain higher mobility. Planar alignment is favorable at the surface, enabling anchoring transition to planar alignment, and then the planar domains quickly grow downward. This growth occurs at velocity on the order of microns per minute³¹, so they cross the 40 nm thickness in a few seconds. At the heating rate of 1 K/min and 5 minutes between observations, we immediately observe

planar domains at the first acquisition above the glass transition temperature.

The lateral coarsening of orientation domains happens at a much slower rate through bulk diffusion to minimize the interface energy. The domain size can be approximated by the Brownian diffusion length of the molecules during continuous heating:

$$R = \sqrt{4 \int D(T) dt},\tag{2}$$

where D(T) is the temperature dependent diffusivity. For a supercooled liquid, the diffusivity follows the Vogel-Fulcher-Tammann equation³²,

$$D(T) = D_0 \exp\left(-\frac{D_T T_0}{T(t) - T_0}\right),\tag{3}$$

where D_0 is high temperature diffusivity, D_T is the fragility and T_0 is the VFT temperature. Knowing the heating profile T(t), we can fit Eqn. 2 and 3 to the experimentally acquired domain size. The model is only fitted to the size of the LC domains measured from 400 K to 425 K. The fitting results are shown in Fig. 3a, with fitting parameters $D_T = 2.67 \pm 0.5$, $T_0 = 328 \pm 60$ K and $D_0 = 5.5 \pm 5.0 \times 10^3$ nm²s⁻¹. D_0 has large uncertainty due to limited temperature range of experimental data. The relaxation time can be estimated from D using the Debye-Stokes-Einstein relation³³, $\tau = ra/6D$, where r = 0.75 nm is the radius of a phenanthroperylene-ester molecule, and a is the thickness approximated by the π - π distance. Fig. 3b plots the inferred $\tau(T)$ with estimated error, along with $\tau(T)$ for three different relaxation modes of phenanthroperylene-ester from other experiments: the bulk α -relaxation τ_{α} , the bulk relaxation related to molecular tumbling au_δ ³⁴, and the surface lpha-relaxation au_s ¹⁹. au_lpha and au_δ are fitted with VFT equation, and au_s is fitted with an Arrhenius function due to the data's lack of curvature. All fitted lines are extrapolated up to 10 K above and below the measurement temperature ranges. The τ governing domain coarsening agrees very well with τ_{α} in the temperature range of measurements, while the extrapolated τ_{s} and τ_{δ} would differ from the domain coarsening τ by orders of magnitidue. VFT fitting parameters for τ_{α} are $D_T = 2.01 \pm 0.3$ and $T_0 = 329 \pm 6$ K, which are within the uncertainty of the same parameters for the domain coarsening τ. with domain size data in this work. This suggests that the slow coarsening of orientation domain is controlled by bulk mass transport process. This result stands in contrast to the lateral size of domains formed during film deposition at elevated substrate temperature, which depends on τ_s^{22} .

139 140

141

142

143

144145

146

147

148

149150

151152

153

154

155

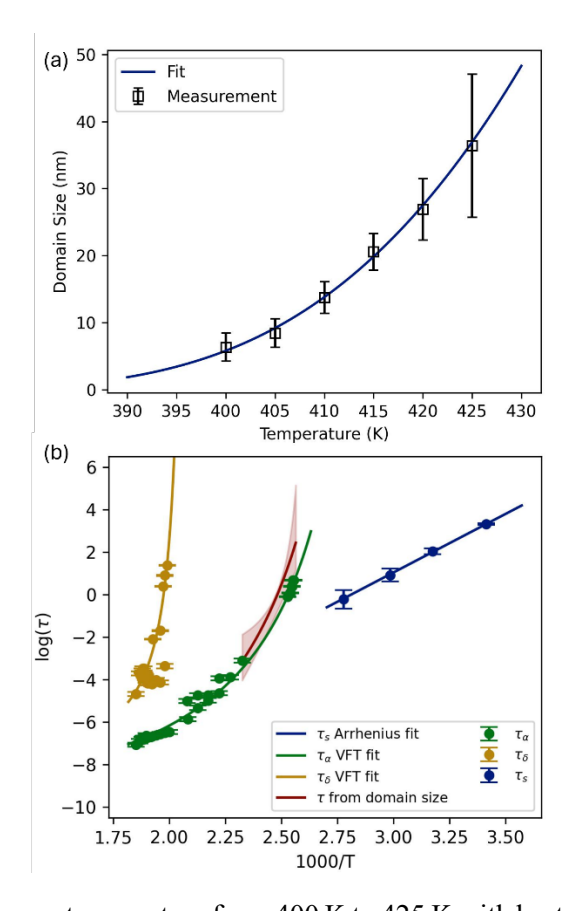


Figure 3. (a) Domain sizes versus temperature from 400 K to 425 K with best fit of a diffusion-based model. Error bars are the same as Fig. 2a. (b) Relaxation times and their temperature dependencies for the bulk α -and δ -relaxation and the surface α -relaxation, overlayed with estimated relaxation time vs. temperature from the domain sizes measurement. Data and errors are replotted from [33] and [19].

The sudden increase of orientation domain size at 430 K and above is accompanied by partial crystallization. As shown in Fig. 1c, sharp crystalline diffraction spots are observed in some regions in the larger domains at and above 430 K. Fig. 4a-c shows more examples of such diffraction patterns. While the crystal structure of crystalline phenanthroperylene-ester has not been comprehensively determined, crystalline diffraction spots are observed in 4D STEM at the same wavevectors as the crystalline peaks in X-ray diffraction experiments on bulk phenanthroperylene-ester crystals. Fig. 4d shows the XRD profiles of a phenanthroperylene-ester glass undergoing crystallization during heating. The liquid crystalline sample crystallized above 402 K. The π - π peak of the LC vanishes and is replaced by a sharper crystalline diffraction peak at higher k. The same effect can be observed in the *in situ* 4D STEM data for PVD thin film, as shown in Fig. 4e. Diffraction spots at k = 0.214 and 0.152 Å⁻¹ as labeled in Fig. 4a-c also have corresponding peaks in the powder XRD profile of the crystal in Fig. 4d. Therefore, the patterns in Fig. 4a-c can be attributed to molecular crystals with different orientations with respect to the electron beam.

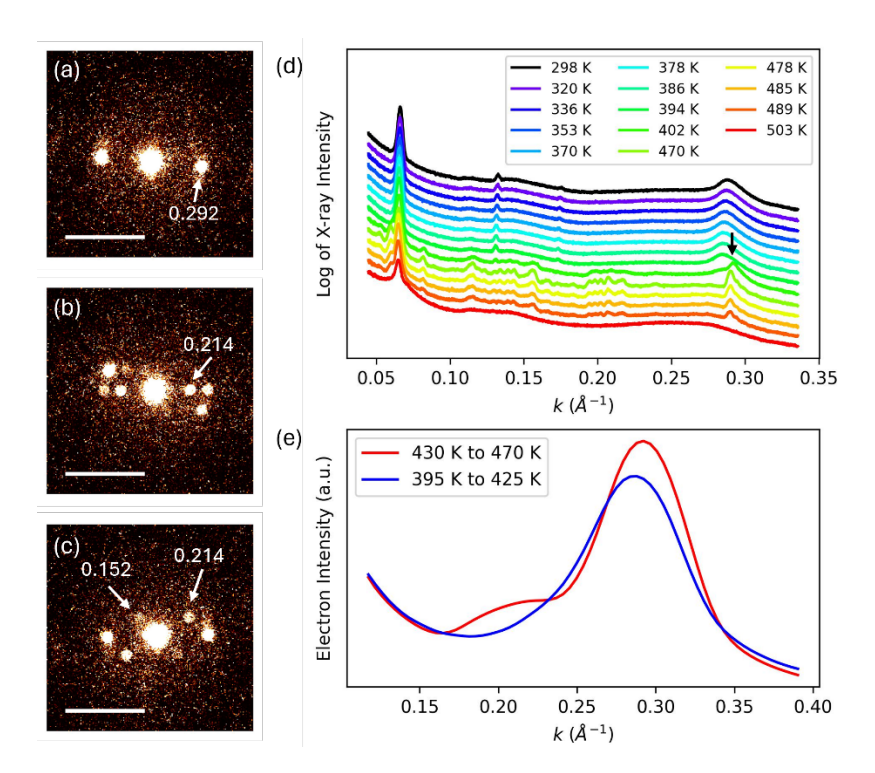


Figure 4. (a-c) Example crystalline diffraction patterns in the 4D STEM datasets at temperatures above 430 K. Scale bars are 0.5 Å⁻¹, and labels are the length of the wavevectors to the corresponding spots in Å⁻¹. (d) XRD profiles at different temperatures for a phenanthroperylene-ester sample that crystallizes during heating. Dark arrow indicates crystalline peak at 402 K and above. (e) Azimuthally averaged diffraction intensity profiles of the 4D STEM data between 395 K to 425 K and 430 to 470 K.

Fig. 5a shows the area fraction of the LC phase and the crystal phase in each scan region at all temperatures measured, derived by classifying the diffraction patterns into sets of arcs or spots. The film partially crystallized starting from 430 K. Interestingly, the area fraction of crystals peaked at 450 K at ~ 50% before decreasing and almost completely vanishing at 480 K, suggesting the crystals melt and transform to LC again at higher temperature. This phenomenon is further confirmed by the average electron diffraction intensity profiles shown in Fig. 5b. Below 400 K, a broad amorphous peak is observed at 0.285 Å⁻¹ marked by the gray arrow, corresponding to the mean aromatic core distance at ~ 3.5 Å, and the film is glassy. From 400 K to 425 K, a moderately narrower π - π peak develops as indicated by the blue arrow, with its peak position shifting to 0.288 Å⁻¹, due to increase of ordering and density during the transition from the glass to the non-glassy LC. At 430 K, a sharp crystalline (001) peak is seen at 0.292 Å⁻¹ (red arrow) along with a weaker peak at 0.214 Å⁻¹ (orange arrow) attributed to the side chains³⁵. The partially crystallized film melts above 460 K as these two crystalline peaks attenuate and vanish at 480 K. The intensity profile at 480 K is similar to the LC diffraction at 400 K to 425 K. Differential scanning calorimetry (DSC) measurements on bulk phenanthroperylene-ester reported similar phase behavior during heating³⁴, with a crystallization onset temperature near 440 K and a melting temperature near 480 K. The lower crystallization and melting temperatures observed in this work compared to bulk DSC measurements could be a result of a combination of the Gibbs-Thompson confinement effect and a 5% temperature uncertainty in the *in situ* heating stage.

174

175

176

177

178

179

180

181

182

183 184

185

186

187

188

189

190

191

192

193 194

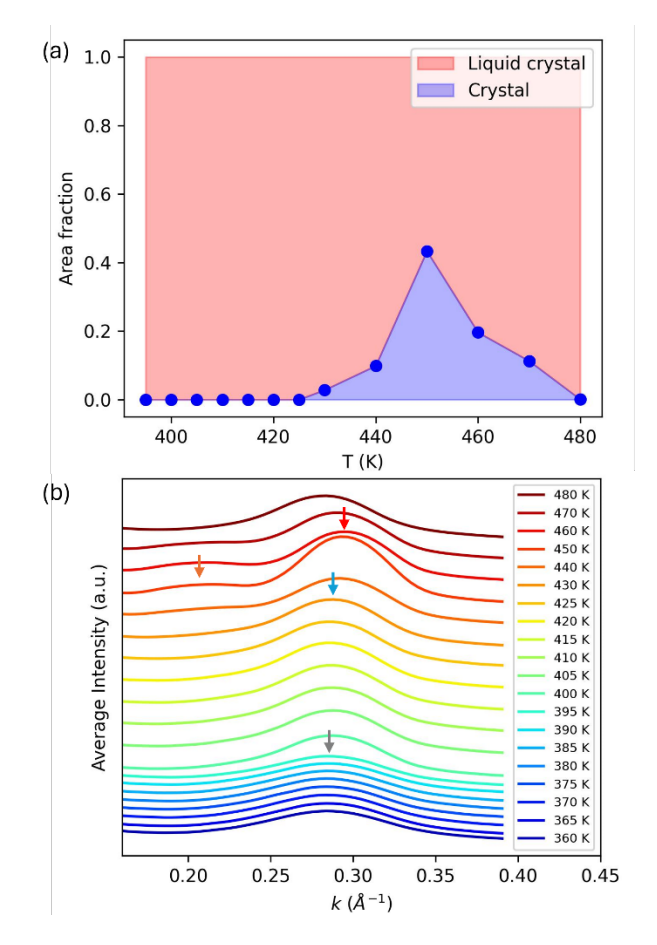


Figure 5. (a) Area fractions of LC and crystalline regions in the field of view as a function of temperature. Blue points are measurements from diffraction pattern classification. (b) Average radial electron diffraction intensity profile of the 4D STEM data at each temperature. Colored arrows are described in the main text.

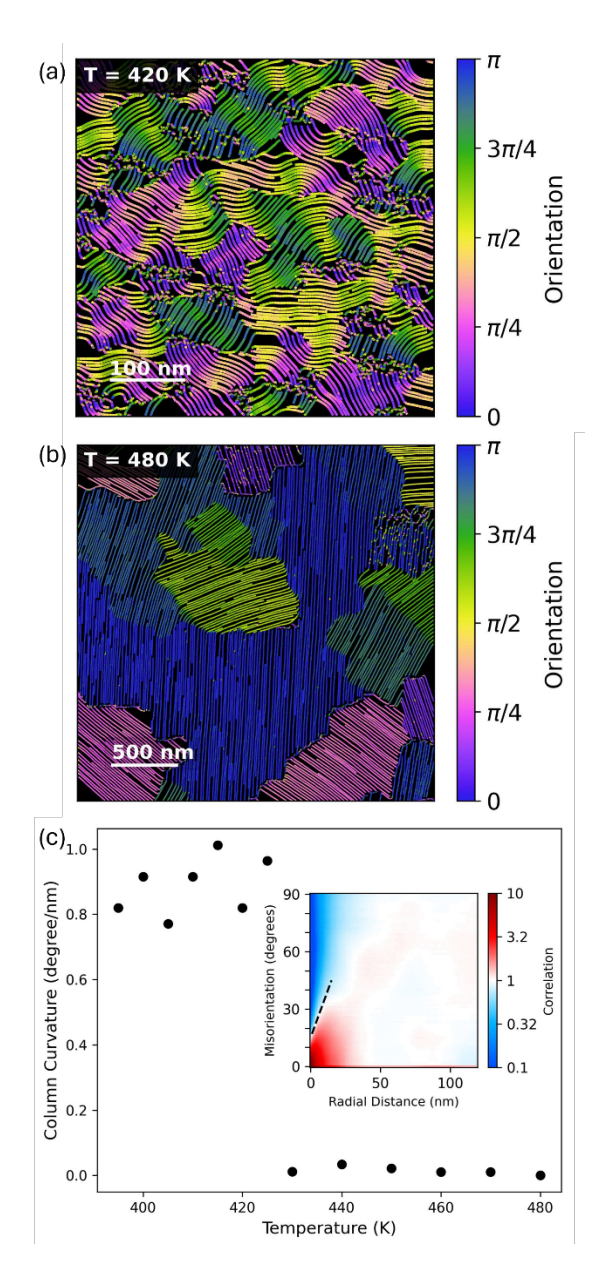


Figure 6. Flowline maps of column orientation at (a) 420 K and (b) 480 K. (c) Intradomain curvature of molecular columns at different temperatures. Inset in (c) shows the orientation correlation function at 425 K, and dashed line indicates random correlation band, the slope of which represents the column curvature.

Although the average diffraction (and therefore structure) is similar between the low temperature (400 K to 425 K) and high temperature (above 480 K) LCs, their microtextures are different. Fig. 6a and 6b show flowline maps³⁰ of the column orientation measured at 420 K and 480 K, respectively. The lines in these maps are orientated along the direction of continuously π - π stacked molecular columns, while the positions and density of the lines do not quantitatively represent the intermolecular spacings. For the low temperature LC at 420 K, the molecular columns are curved, and the field exhibits notable LC defects like disclinations³⁶. In contrast, the high temperature LC at 480 K has straight molecular columns and sharp orientation transitions between domains. The curvature of molecular columns inside each orientation domain can be quantified by the slope of random correlation band in the orientation correlation function³⁰, as illustrated in the inset in Fig. 6c. Fig. 6c shows the estimated column curvature at each temperature. At and below 425

215 K, molecular columns have curvatures ranging from $0.8 \sim 1.0$ degree per nm, with small, random variation 216 with temperature. Starting from 430 K, which is the crystallization onset temperature, the column curvature nearly vanishes, and it stays extremely small even after the transition back to the LC phase at 460 K. At 217 218 480 K, even though the film is in LC phase, the molecular column stays uniform within each orientation domain. While LC phases tend to bend molecular columns to minimize interfaces³⁷, the high temperature 219 LCs observed here seem to inherit their mesoscale structures from the molecular arrangement of crystals at 220 lower temperature, therefore retaining their crystal-like molecular columns and orientation domains that 221 reflect crystalline grains. 222

The planar domain texture observed in the high temperature LC in this work is unlike any previously reported as-prepared columnar LC thin films in planar alignment, either via spin-coating³⁸, PVD deposition³⁹, or cooling from the isotropic liquid²². In particular, in our previous work on phenanthroperylene-ester²², we studied a film that start in disordered glassy state, then was heated rapidly (150 K/min) into the LC state at 457 K, then cooled to room temperature at 2.5 K/min. The orientation correlation function data form this film (Fig 3d in Ref. 22) shows a similar domain size to what we observe here starting at 450 K, but the curvature is 0.35 degrees / nm. That is less than we observe in the LC state derived from the glass (below 425 K), but significantly larger than the LC phase derived from the crystal above 460 K. While macroscopically uniform homeotropic thin films have been obtained up to millimeters in size^{40,41}, planar orientation is always accompanied by bending of columns or defects, at least on the macroscopic length scale. The results from this work suggest that LC domains obtained from heating up a glassy thin film that crystallized midway retain the highly uniform crystal-like orientation over the scale of the crystal's grain size, and this organization likely can solidify upon cooling through glass transition²². This result points to a potential new approach of fabrication and processing of LC thin films to obtain uniform orientation at larger length scales through an intermediate single crystal, although significant additional work to control the nucleation density and size of the intermediate crystals would be required to obtain large domains.

Conclusion

223

224

225226

227228

229

230

231232

233

234

235236

237

238239

240

241

242

243

244

245

246247

248249

250

251252

253

254

In summary, we have characterized with nanometer resolution the planar realignment and domain growth of an initially disordered columnar liquid crystal using *in-situ* 4D STEM. When heated above the glass transition temperature, roughly 6 nm planar domains of the phenanthroperylene-ester film grew quickly through the film thickness, followed by lateral growth at a much slower rate. Using a Brownian diffusion model, the lateral domain growth is determined to be controlled by bulk diffusion with VFT diffusivity temperature dependence. The film went through a complex phase behavior of partial crystallization and melting upon further heating. We observed a columnar LC phase at the highest temperature with a distinct intradomain microstructure comprised of unusually straight columns of molecules separated by sharp boundaries. This behavior may suggest a processing path to highly oriented columnar LCs using a crystal phase as an intermediate step, which could have significant implication in fabrication of nanostructured LCs used in semiconductor devices. 4D STEM measurement provides nanometer scale ordering information that offers great opportunity to further our understanding of reorientation and domain reorganization mechanisms.

Methods

- 255 Sample preparation
- 256 Phenanthroperylene-ester glasses were deposited onto TEM heating chips (DENS Wildfire) with a thin
- 257 electron transparent SiN_x membrane. Fresh nano-chips were cleaned with acetone before deposition. Then
- 258 the nano-chip was affixed to one side of a galvanized iron plate using magnets. Subsequently, thermal paste

- (Apiezon H) was smeared between the opposite side of the galvanized iron plate and copper blocks that were maintained at the desired substrate temperature using a LakeShore 336 PID controller, resistive cartridge heaters, and platinum resistive temperature detectors. Deposition is performed in a high vacuum chamber with a base pressure of 10^{-7} Torr. 40 nm phenanthroperylene-ester films were deposited at a deposition rate of 0.6 ± 0.1 Å/s, monitored with a quartz crystal microbalance (QCM), and a substrate temperature of 340 K. The film thickness was confirmed by its elastic electron transmittance. Based on prior work¹⁹, this set of conditions produces non-hexagonal random packing of π - π stacking columns, with
- a distribution of molecular orientations close to planar alignment.
- 267 In situ 4D STEM measurements
- The experiments are performed at 200 kV in a FEI Titan G2 microscope operated in micro-probe EFSTEM
- mode. The probe convergence angle was 0.7 mrad, with a 10 µm C2 aperture, generating a probe current of 4.3 pA. Data is collected using a Direct Electron Celeritas detector with a 256 by 256 readout area. A
- camera length of 1700 mm is used making the detector pixel size 0.00475 Å⁻¹. The 4D STEM orientation
- 272 mapping method and data analysis are described in ²².
- 273 The sample was loaded into a heating holder (DENS Wildfire) and heated to 360 K before start of
- acquisition. The sample temperature was ramped up at a heating rate of 1 K/min from 360 K to 480 K. The
- 275 film starts to evaporate inside the microscope vacuum at temperatures higher than 480 K. The absolute
- value of sample temperature has an error of up to 5% due to instrument uncertainty. To accommodate
- 277 different domain sizes at different temperatures, 4D STEM data were acquired every 5 K from 360 K to
- 425 K using a 498 by 498 nm scan field of view and then every 10 K from 430 K to 480 K using a 2.79 by
- 2.79 µm field of view. Scanning array sizes are 240 by 240 pixels and 640 by 640 pixels respectively. All
- data were acquired at a readout rate of 4000 frames. Acquisitions take 14.4 seconds at lower temperatures
- and 102.4 seconds at higher temperatures. At a heating rate of 1 K/min, these acquisitions can be viewed as
- measurements of the quasistatic mesoscale structure of the sample at the corresponding temperature.
- However, the samples were not necessarily in thermal equilibrium at each temperature. Due to the effects
- of beam damage as discussed in the Supplementary Information, a new region of the sample was imaged at
- every temperature. As a result, only changes in the distribution of domain sizes and related microstructure
- were measured, not the change in size of individual domains with time and temperature.
- 287 *X-ray scattering*
- 288 X-ray diffraction (XRD) experiments were conducted using a Bruker D8 Discover diffractometer on a bulk
- powder sample of glassy phenanthroperylene-ester. The glassy sample preparation procedure is detailed in
- 290 ³⁵. Phenanthroperylene-ester powder was filled into an X-ray transmitting capillary tube, melted, vitrified,
- and then heated using an Instec mK2000 heating stage from room temperature up to 503 K. The sample in
- a capillary tube was illuminated perpendicularly, and the scattered x rays were measured in the transmission
- geometry. The area detector was placed off-center at $2\theta = 20^{\circ}$ and 20 cm from the sample to allow coverage
- geometry. The discrete was placed on center at 20 and 20 cm from the sample to allow coverage
- of k (=2sin θ/λ) range from 0.048 to 0.334 Å⁻¹. At each measurement temperature, the sample was
- equilibrated for 5 min and measured for 5 min. The two-dimensional x-ray scattering data were integrated
- using the software Datasqueeze to yield a one-dimensional intensity vs k plot.

Acknowledgements

- 299 This work was entirely supported by the Wisconsin Materials Research Science and Engineering Center.
- Primary experiments and data analysis were supported by DMR-1720415. Final experiments, analysis and

297

- 301 manuscript preparation were supported by DMR-2309000. The authors thank Dr Joonatan Laulainen for
- the discussion about orientation analysis. The authors gratefully acknowledge the use of facilities and 302
- instrumentation supported by the Wisconsin Materials Research Science and Engineering Center (DMR-303
- 1720415 and DMR-2309000). 304

305 **Supporting Information Available**

- 306 Discussion on the effect of electron beam damage on 4D STEM orientation mapping results; orientation
- 307 maps from repeated 4D STEM experiment in room temperature and in situ conditions displaying the effect
- of beam damage; additional orientation mapping results during continuous heating; orientation correlation 308
- function of the mapping results; illustration of domain size estimation using the orientation correlation 309
- function. 310

311 **Data Availability**

- Raw and processed data for in situ 4D STEM and XRD, and the data plotted in the figures are available 312
- 313 through the Materials Data Facility (DOI will be provided upon acceptance).

314 Reference

- Eccher, J.; Zajaczkowski, W.; Faria, G. C.; Bock, H.; von Seggern, H.; Pisula, W.; Bechtold, I. H. 315 (1)
- 316 Thermal Evaporation versus Spin-Coating: Electrical Performance in Columnar Liquid Crystal
- OLEDs. ACS Appl. Mater. Interfaces 2015, 7 (30), 16374–16381. 317
- https://doi.org/10.1021/acsami.5b03496. 318
- 319 (2) Sutton, C.; Risko, C.; Brédas, J.-L. Noncovalent Intermolecular Interactions in Organic Electronic
- Materials: Implications for the Molecular Packing vs Electronic Properties of Acenes. Chem. 320
- 321 Mater. 2016, 28 (1), 3–16. https://doi.org/10.1021/acs.chemmater.5b03266.
- Zheng, Y.-Q.; Zhang, J.; Yang, F.; Komino, T.; Wei, B.; Zhang, J.; Wang, Z.; Pu, W.; Yang, C.; 322 (3)
- Adachi, C. Influence of Deposition Substrate Temperature on the Morphology and Molecular 323
- Orientation of Chloroaluminum Phthalocyanine Films as Well the Performance of Organic 324
- Photovoltaic Cells. Nanotechnology 2015, 26 (40), 405202. https://doi.org/10.1088/0957-325
- 326 4484/26/40/405202.
- **(4)** Yokoyama, D.; Setoguchi, Y.; Sakaguchi, A.; Suzuki, M.; Adachi, C. Orientation Control of 327
- Linear-Shaped Molecules in Vacuum-Deposited Organic Amorphous Films and Its Effect on 328
- Carrier Mobilities. Adv. Funct. Mater. 2010, 20 (3), 386–391. 329
- https://doi.org/https://doi.org/10.1002/adfm.200901684. 330
- 331 (5) Termine, R.; Golemme, A. Charge Mobility in Discotic Liquid Crystals. Int. J. Mol. Sci. 2021, 22
- (2), 877. https://doi.org/10.3390/ijms22020877. 332
- Street, R. A.; Northrup, J. E.; Salleo, A. Transport in Polycrystalline Polymer Thin-Film 333 (6)
- Transistors. Phys. Rev. B 2005, 71 (16), 165202. https://doi.org/10.1103/PhysRevB.71.165202. 334
- 335 (7) Noguchi, Y.; Miyazaki, Y.; Tanaka, Y.; Sato, N.; Nakayama, Y.; Schmidt, T. D.; Brütting, W.;
- Ishii, H. Charge Accumulation at Organic Semiconductor Interfaces Due to a Permanent Dipole 336
- Moment and Its Orientational Order in Bilayer Devices. J. Appl. Phys. 2012, 111 (11), 114508. 337
- https://doi.org/10.1063/1.4724349. 338
- Kim, D. S.; Čopar, S.; Tkalec, U.; Yoon, D. K. Mosaics of Topological Defects in Micropatterned 339 (8) 340 Liquid Crystal Textures. Sci. Adv. 2018, 4 (11), 1–8. https://doi.org/10.1126/sciadv.aau8064.

- 341 (9) Kobashi, J.; Yoshida, H.; Ozaki, M. Planar Optics with Patterned Chiral Liquid Crystals. *Nat. Photonics* **2016**, *10* (6), 389–392. https://doi.org/10.1038/nphoton.2016.66.
- 343 (10) Bagchi, K.; Emeršič, T.; Wang, Z.; Chen, W.; Kim, M.; Eom, C.; Jiang, Z.; Strzalka, J.; de Pablo,
 344 J. J.; Nealey, P. F. Crystalline Solid Retains Memory of Anisotropy in Precursor Liquid
 345 Crystalline Phase. J. Mater. Chem. C 2023, 11 (34), 11466–11475.
 346 https://doi.org/10.1039/d3tc01175e.
- 347 (11) Simpson, C. D.; Wu, J.; Watson, M. D.; Müllen, K. From Graphite Molecules to Columnar 348 Superstructures – an Exercise in Nanoscience. *J. Mater. Chem.* **2004**, *14* (4), 494–504. 349 https://doi.org/10.1039/B312789C.
- Woltman, S. J.; Jay, G. D.; Crawford, G. P. Liquid-Crystal Materials Find a New Order in Biomedical Applications. *Nat. Mater.* **2007**, *6* (12), 929–938. https://doi.org/10.1038/nmat2010.
- Fleischmann, E.-K.; Zentel, R. Liquid-Crystalline Ordering as a Concept in Materials Science: From Semiconductors to Stimuli-Responsive Devices. *Angew. Chemie Int. Ed.* **2013**, *52* (34), 8810–8827. https://doi.org/https://doi.org/10.1002/anie.201300371.
- Lagerwall, J. P. F.; Scalia, G. A New Era for Liquid Crystal Research: Applications of Liquid
 Crystals in Soft Matter Nano-, Bio- and Microtechnology. Curr. Appl. Phys. 2012, 12 (6), 1387–
 1412. https://doi.org/https://doi.org/10.1016/j.cap.2012.03.019.
- Nunes da Silva, F.; Marchi Luciano, H.; Stadtlober, C. H.; Farias, G.; Durola, F.; Eccher, J.;
 Bechtold, I. H.; Bock, H.; Gallardo, H.; Vieira, A. A. Dissymmetric Triaryltriazines: Small Mass
 Columnar Glasses. *Chem. A Eur. J.* 2023, 29 (46), e202301319.
 https://doi.org/https://doi.org/10.1002/chem.202301319.
- Tarnacka, M.; Adrjanowicz, K.; Kaminska, E.; Kaminski, K.; Grzybowska, K.; Kolodziejczyk, K.;
 Wlodarczyk, P.; Hawelek, L.; Garbacz, G.; Kocot, A.; Paluch, M. Molecular Dynamics of
 Itraconazole at Ambient and High Pressure. *Phys. Chem. Chem. Phys.* 2013, *15* (47), 20742–
 20752. https://doi.org/10.1039/C3CP52643G.
- 366 (17) Farias, G.; Simeão, D. S.; Moreira, T. S.; dos Santos, P. L.; Bentaleb, A.; Girotto, E.; Monkman,
 367 A. P.; Eccher, J.; Durola, F.; Bock, H.; de Souza, B.; Bechtold, I. H. An Unusual Plank-Shaped
 368 Nematogen with a Graphene Nanoribbon Core. *J. Mater. Chem. C* 2019, 7 (39), 12080–12085.
 369 https://doi.org/10.1039/C9TC03704G.
- 370 (18) Bagchi, K.; Ediger, M. D. Controlling Structure and Properties of Vapor-Deposited Glasses of 371 Organic Semiconductors: Recent Advances and Challenges. *J. Phys. Chem. Lett.* **2020**, *11* (17), 372 6935–6945. https://doi.org/10.1021/acs.jpclett.0c01682.
- 373 (19) Bishop, C.; Chen, Z.; Toney, M. F.; Bock, H.; Yu, L.; Ediger, M. D. Using Deposition Rate and Substrate Temperature to Manipulate Liquid Crystal-like Order in a Vapor-Deposited Hexagonal Columnar Glass. *J. Phys. Chem. B* **2021**, *125* (10), 2761–2770. https://doi.org/10.1021/acs.jpcb.0c11564.
- 377 (20) Gujral, A.; Gómez, J.; Ruan, S.; Toney, M. F.; Bock, H.; Yu, L.; Ediger, M. D. Vapor-Deposited 378 Glasses with Long-Range Columnar Liquid Crystalline Order. *Chem. Mater.* **2017**, *29* (21), 9110– 379 9119. https://doi.org/10.1021/acs.chemmater.7b02852.
- 380 (21) Grelet, E.; Bock, H. Control of the Orientation of Thin Open Supported Columnar Liquid Crystal 381 Films by the Kinetics of Growth. *Europhys. Lett.* **2006**, *73* (5), 712–718. 382 https://doi.org/10.1209/epl/i2005-10459-5.

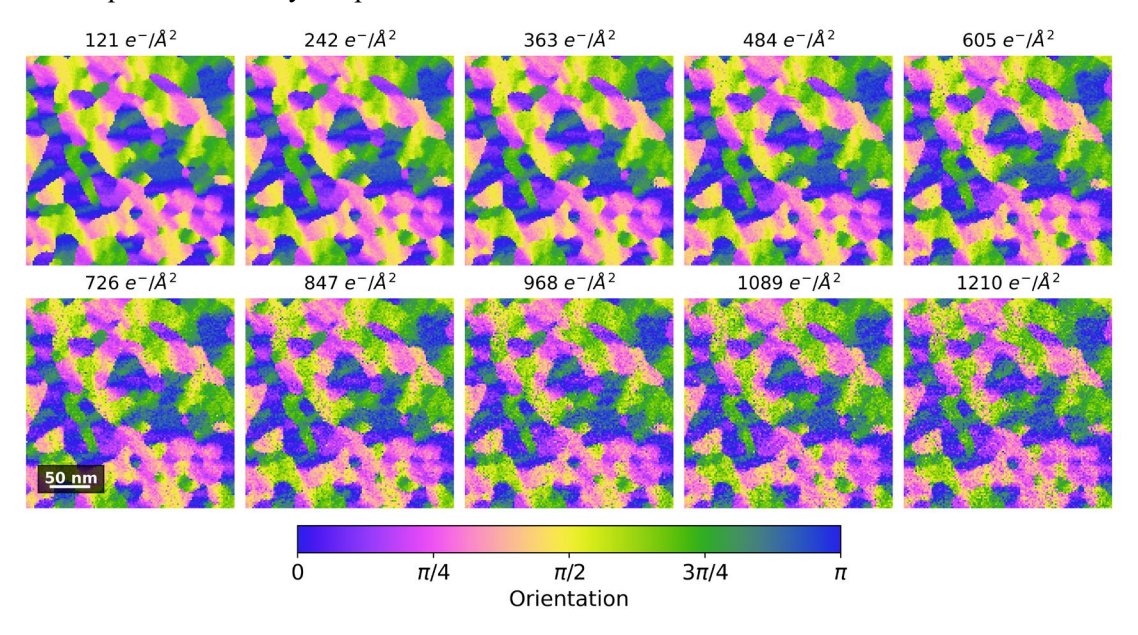
- Chatterjee, D.; Huang, S.; Gu, K.; Ju, J.; Yu, J.; Bock, H.; Yu, L.; Ediger, M. D.; Voyles, P. M. Using 4D STEM to Probe Mesoscale Order in Molecular Glass Films Prepared by Physical Vapor Deposition. *Nano Lett.* **2023**, *23* (5), 2009–2015. https://doi.org/10.1021/acs.nanolett.3c00197.
- 386 (23) Bisoyi, H. K.; Li, Q. Stimuli Directed Alignment of Self-Organized One-Dimensional
 387 Semiconducting Columnar Liquid Crystal Nanostructures for Organic Electronics. *Prog. Mater.* 388 Sci. 2019, 104, 1–52. https://doi.org/https://doi.org/10.1016/j.pmatsci.2019.03.005.
- Kang, S.-W.; Li, Q.; Chapman, B. D.; Pindak, R.; Cross, J. O.; Li, L.; Nakata, M.; Kumar, S.
 Microfocus X-Ray Diffraction Study of the Columnar Phase of Porphyrin-Based Mesogens.
 Chem. Mater. 2007, 19 (23), 5657–5663. https://doi.org/10.1021/cm702063a.
- Huang, S.; Francis, C.; Sunderland, J.; Jambur, V.; Szlufarska, I.; Voyles, P. M. Large Area, High
 Resolution Mapping of Approximate Rotational Symmetries in a Pd77.5Cu6Si16.5 Metallic Glass
 Thin Film. *Ultramicroscopy* 2022, 241, 113612.
 https://doi.org/https://doi.org/10.1016/j.ultramic.2022.113612.
- Liu, A. C. Y.; Neish, M. J.; Stokol, G.; Buckley, G. A.; Smillie, L. A.; De Jonge, M. D.; Ott, R. T.;
 Kramer, M. J.; Bourgeois, L. Systematic Mapping of Icosahedral Short-Range Order in a Melt Spun Zr 36Cu64 Metallic Glass. *Phys. Rev. Lett.* 2013, *110* (20), 1–5.
 https://doi.org/10.1103/PhysRevLett.110.205505.
- 400 (27) Chatterjee, D.; Wei, J.; kvit, A.; Bammes, B.; Levin, B.; Bilhorn, R.; Voyles, P. An Ultrafast
 401 Direct Electron Camera for 4D STEM. *Microsc. Microanal.* 2021, 27 (S1), 1004–1006.
 402 https://doi.org/DOI: 10.1017/S1431927621003809.
- Johnstone, D. N.; Firth, F. C. N.; Grey, C. P.; Midgley, P. A.; Cliffe, M. J.; Collins, S. M.;
 Johnstone, D. N. Direct Imaging of Correlated Defect Nanodomains in a Metal-Organic
 Framework. J. Am. Chem. Soc. 2020, 142 (30), 13081–13089.
 https://doi.org/10.1021/jacs.0c04468.
- 407 (29) Bustillo, K. C.; Zeltmann, S. E.; Chen, M.; Donohue, J.; Ciston, J.; Ophus, C.; Minor, A. M. 4D 408 STEM of Beam-Sensitive Materials. *Acc. Chem. Res.* 2021, 54 (11), 2543–2551.
 409 https://doi.org/10.1021/acs.accounts.1c00073.
- 410 (30) Panova, O.; Ophus, C.; Takacs, C. J.; Bustillo, K. C.; Balhorn, L.; Salleo, A.; Balsara, N.; Minor,
 411 A. M. Diffraction Imaging of Nanocrystalline Structures in Organic Semiconductor Molecular
 412 Thin Films. *Nat. Mater.* 2019, *18* (8), 860–865. https://doi.org/10.1038/s41563-019-0387-3.
- 413 (31) Brunet, T.; Thiebaut, O.; Charlet, É.; Bock, H.; Kelber, J.; Grelet, É. Anchoring Transition in 414 Confined Discotic Columnar Liquid Crystal Films. *Epl* **2011**, *93* (1), 16004. 415 https://doi.org/10.1209/0295-5075/93/16004.
- 416 (32) Ediger, M. D.; Angell, C. A.; Nagel, S. R. Supercooled Liquids and Glasses. *J. Phys. Chem.* **1996**, 417 *100* (31), 13200–13212. https://doi.org/10.1021/jp953538d.
- 418 (33) Lavalette, D.; Tétreau, C.; Tourbez, M.; Blouquit, Y. Microscopic Viscosity and Rotational
 419 Diffusion of Proteins in a Macromolecular Environment. *Biophys. J.* **1999**, *76* (5), 2744–2751.
 420 https://doi.org/10.1016/S0006-3495(99)77427-8.
- 421 (34) Chen, Z.; Bishop, C.; Thoms, E.; Bock, H.; Ediger, M. D.; Richert, R.; Yu, L. Controlling the
 422 Columnar Order in a Discotic Liquid Crystal by Kinetic Arrest of Disc Tumbling. *Chem. Mater.*423 **2021**, *33* (12), 4757–4764. https://doi.org/10.1021/acs.chemmater.1c01331.

- 424 (35) Yu, J.; Chen, Z.; Fatina, C.; Chatterjee, D.; Bock, H.; Richert, R.; Voyles, P.; Ediger, M. D.; Yu, L. Engineering the Glass Structure of a Discotic Liquid Crystal by Multiple Kinetic Arrests. *J. Chem. Phys.* **2023**, *158* (20). https://doi.org/10.1063/5.0149886.
- 427 (36) Chandrasekhar, S.; Ranganath, G. S. The Structure and Energetics of Defects in Liquid Crystals.
 428 Adv. Phys. 1986, 35 (6), 507–596. https://doi.org/10.1080/00018738600101941.
- 429 (37) Tschierske, C. Liquid Crystal Engineering New Complex Mesophase Structures and Their 430 Relations to Polymer Morphologies, Nanoscale Patterning and Crystal Engineering. *Chem. Soc.* 431 *Rev.* 2007, 36 (12), 1930–1970. https://doi.org/10.1039/b615517k.
- 432 (38) Eccher, J.; Faria, G. C.; Bock, H.; Von Seggern, H.; Bechtold, I. H. Order Induced Charge Carrier
 433 Mobility Enhancement in Columnar Liquid Crystal Diodes. *ACS Appl. Mater. Interfaces* **2013**, 5
 434 (22), 11935–11943. https://doi.org/10.1021/am403681q.
- 435 (39) Grelet, E.; Dardel, S.; Bock, H.; Goldmann, M.; Lacaze, E.; Nallet, F. Morphology of Open Films
 436 of Discotic Hexagonal Columnar Liquid Crystals as Probed by Grazing Incidence X-Ray
 437 Diffraction. Eur. Phys. J. E 2010, 31 (4), 343–349. https://doi.org/10.1140/epje/i2010-10586-2.
- Charlet, E.; Grelet, E.; Brettes, P.; Bock, H.; Saadaoui, H.; Cisse, L.; Destruel, P.; Gherardi, N.;
 Seguy, I. Ultrathin Films of Homeotropically Aligned Columnar Liquid Crystals on Indium Tin
 Oxide Electrodes. *Appl. Phys. Lett.* 2008, 92 (2), 1–4. https://doi.org/10.1063/1.2831009.
- 441 (41) Monobe, H.; Awazu, K.; Shimizu, Y. Alignment Control of a Columnar Liquid Crystal for a
 442 Uniformly Homeotropic Domain Using Circularly Polarized Infrared Irradiation. *Adv. Mater.* 443 2006, 18 (5), 607–610. https://doi.org/https://doi.org/10.1002/adma.200501762.

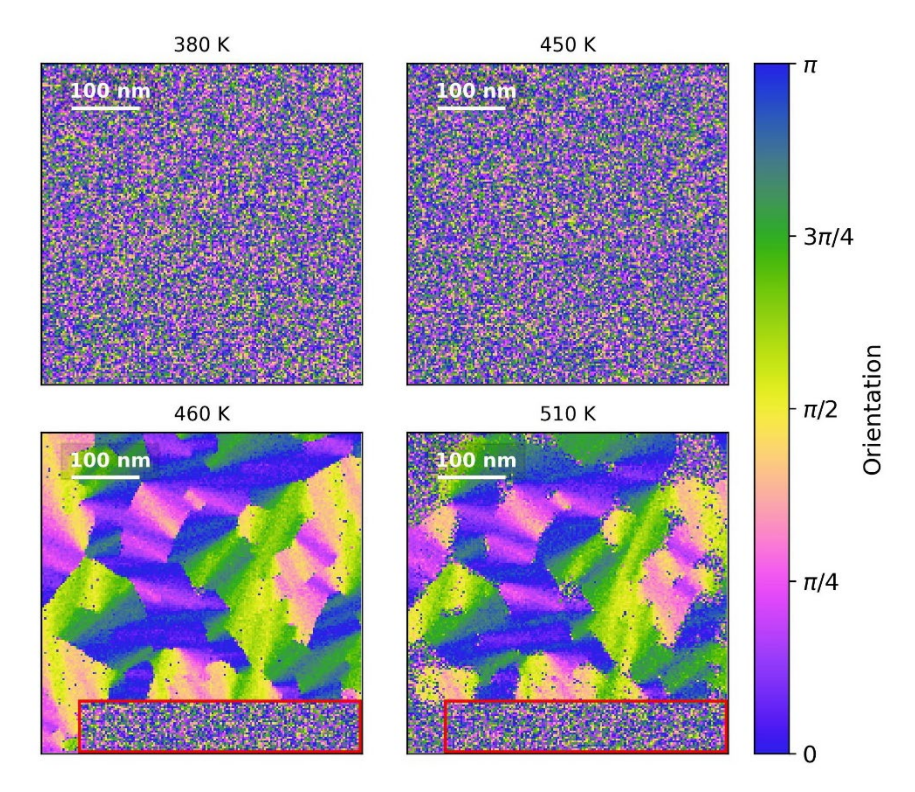
Effect of electron beam damage

We performed an initial set of experiments to identify conditions under which reliable data could be acquired considering the impact of beam damage. The effects of beam damage were studied by repeated acquisition on a single region of a sample with planar orientation domains at room temperature, as shown in Fig. S1. Mapping results from an area that has been exposed to 1210 e⁻/Å² electron still display full information of the orientation, albeit at an increased level of noise compared to lower dose measurements. Mapping results from initial *in situ* experiments is shown in Fig. S2. At a low dose rate of 27 e⁻/Å² per orientation map, no orientation domains are observed in the fixed field of view up to 450 K. At 460 K, the scanning region was moved to a different area. Large orientation domains can be seen in the previously unilluminated area, but no domains are seen in the previously illuminated area. The orientation maps stay unchanged at higher temperatures after the shift in field of view on the sample.

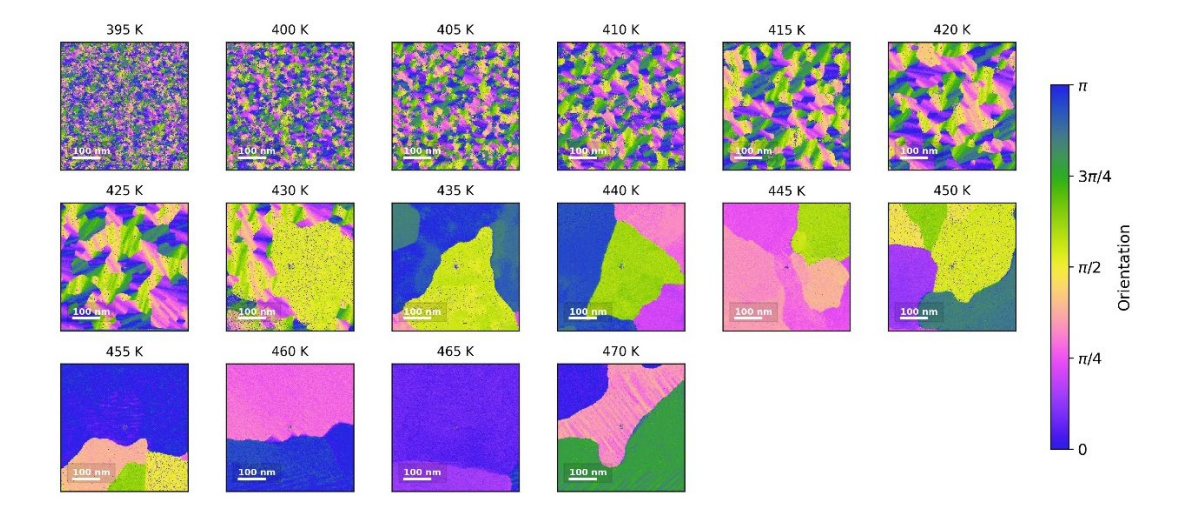
These results demonstrate that even an electron dose that is 2% of the "survivable" dose for static orientation mapping is sufficient to prevent changes in orientation with temperature from developing. Static orientation mapping depends on the sum of all the scattering from pairs of atoms with distances close to the π - π stacking distance of ~3.5 Å. Thus, the peak in the scattering is relatively broad and robust against displacement of atoms by the beam. Thermal orientation ordering depends on the collective realignment of clusters of molecules, so we speculate that if single atoms are displaced by the electron beam, mesoscopic reordering will not occur. These results emphasize that different electron microscopy experiments probing different structural features come with different dose (and damage) thresholds, even for the same molecule. For this work, the a new, previously unexposed region of the sample is selected for 4D STEM acquisition at every temperature.



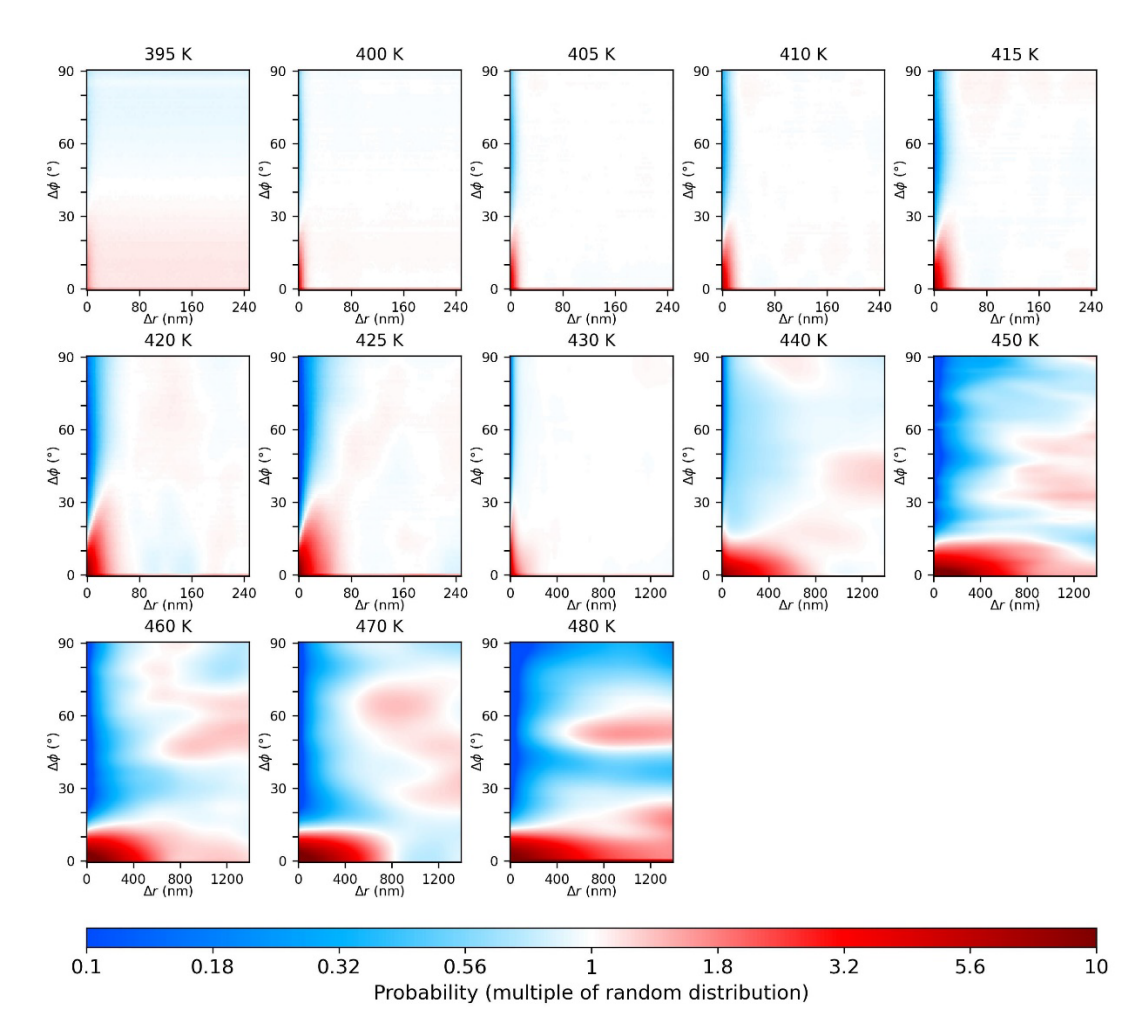
Supplementary Figure 1 Orientation maps from repeated 4D STEM acquisitions on the same region of a phenanthroperylene-ester deposited at 370 K. Information about the orientation domains is preserved up to the highest dose.



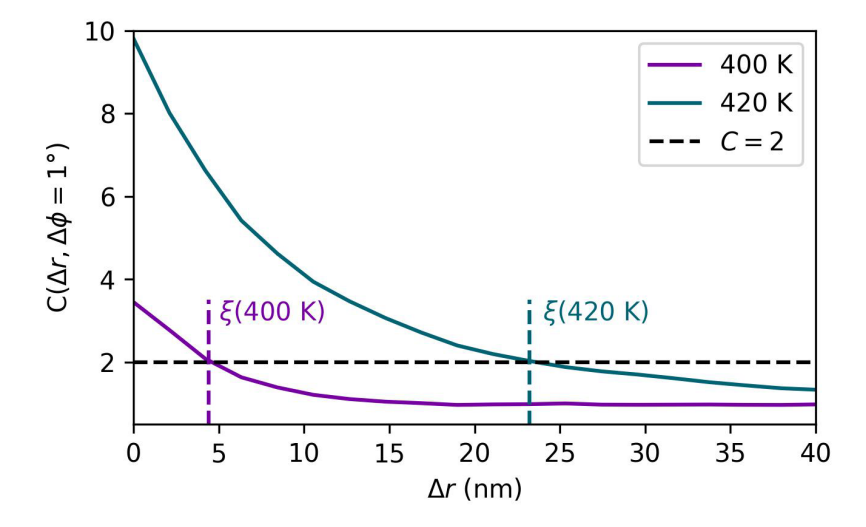
Supplementary Figure 2 "Orientation" maps of phenanthroperylene-ester thin film at four different temperatures acquired during continuous heating, acquired at a low dose of 27 e⁻/Å² per map. From 380 K to 450 K, the same area is illuminated, resulting in no planar self-alignment and random measured "orientation". Above 460 K, another nearby, partially overlapping area was studied. The red rectangle marks the top right corner of the previously illuminated region with no orientation domain, in sharp contrast to the domains formed in the adjacent region which was not previously illuminated. At 510 K and above, thin film evaporates in the microscope column, reflected by the degradation of the orientation map.



Supplementary Figure 3 Orientation maps of the thin film during continuous heating from 395 K to 470 K with a heating rate of 1 K/min. Maps are acquired from different regions at each temperature.



Supplementary Figure 4 Orientation correlation functions calculated from Fig. 1d at every temperature.



Supplementary Figure 5 Orientation correlation functions $C(\Delta r, \Delta \phi = 1^{\circ})$ at 400 K and 420 K, illustrating estimation of domain size ξ .